J|A|C|S
ARTICLES
Published on Web 01/11/2007

New Members of a Class of Iron−Thiolate−Nitrosyl Compounds: Trinuclear Iron−Thiolate−Nitrosyl Complexes Containing Fe_3S_6 Core

I-Jui Hsu,[†] Chung-Hung Hsieh,[‡] Shyue-Chu Ke,*[,§] Kuo-An Chiang,[§] Jenn-Min Lee,[⊥] Jin-Ming Chen,[⊥] Ling-Yun Jang,[⊥] Gene-Hsiang Lee,[†] Yu Wang,*[,†] and Wen-Feng Liaw*[,‡]

Contribution from the Department of Chemistry, National Tsing Hua University, Hsinchu 30013, Taiwan, Department of Chemistry, National Taiwan University, Taipei, Taiwan, Department of Physics, National Dong Hwa University, Hualien, Taiwan, and National Synchroton RaditionResearch Center, Hsinchu, Taiwan

Received July 27, 2006; E-mail: wfliaw@mx.nthu.edu.tw; wangyu@ntu.edu.tw; ke@mail.ndhu.edu.tw

Abstract: The neutral trinuclear iron−thiolate−nitrosyl, $[(ON)Fe(\mu\text{-}S,S\text{-}C_6H_4)]_3$ (**1**), and its oxidation product, $[(ON)Fe(\mu\text{-}S,S\text{-}C_6H_4)]_3[PF_6]$ (**2**), were synthesized and characterized by IR, X-ray diffraction, X-ray absorption, electron paramagnetic resonance (EPR), and magnetic measurement. The five-coordinated, square pyramidal geometry around each iron atom in complex **1** remains intact when complex **1** is oxidized to yield complex **2**. Magnetic measurements and EPR results show that there is only one unpaired electron in complex **1** ($S_{total} = {}^1/_2$) and no unpaired electron ($S_{total} = 0$) in **2**. The detailed geometric comparisons between complexes **1** and **2** provide understanding of the role that the unpaired electron plays in the chemical bonding of this trinuclear complex. Significant shortening of the Fe−Fe, Fe−N, and Fe−S distances around Fe(1) is observed when complex **1** is oxidized to **2**. This result implicates that the removal of the unpaired electron does induce the strengthening of the Fe−Fe, Fe−N, and Fe−S bonds in the Fe(1) fragment. A significant shift of the ν_{NO} stretching frequency from 1751 cm^{-1} (**1**) to 1821, 1857 cm^{-1} (**2**) (KBr) also indicates the strengthening of the N−O bonds in complex **2**. The EPR, X-ray absorption, magnetic measurements, and molecular orbital calculations lead to the conclusion that the unpaired electron in complex **1** is mainly allocated in the Fe(1) fragment and is best described as $\{Fe(1)NO\}^7$, so that the unpaired electron is delocalized between Fe and NO via d−π^* orbital interaction; some contributions from [Fe(2)NO] and [Fe(3)NO] as well as the thiolates associated with Fe (1) are also realized. According to MO calculations, the spin density of complex **1** is predominately located at the Fe atoms with 0.60, −0.15, and 0.25 at Fe(1), Fe(2), and Fe(3), respectively.

Downloaded by NATIONAL TAIWAN UNIV on August 25, 2009 | http://pubs.acs.org
Publication Date (Web): January 11, 2007 | doi: 10.1021/ja065401e

Introduction

Iron−sulfur−nitrosyl complexes have attracted considerable interest stimulated by (i) the reported formation of protein-bound dinitrosyl−iron complexes (DNICs) in the anaerobic reaction of *Chromatium vinosum* high-potential iron protein with nitric oxide,[1,2] (ii) the observation of $[Fe_4S_3(NO)_7]^-$ acting as an inhibitor of *Clostridium sporogenes* in culture medium,[3] (iii) the metal nitrosyl complexes being employed to serve as nitric oxide delivery reagents to biological targets,[4,5] and (iv) the versatile bonding properties between metal and NO.[4−17]

Due to the existence of the potential electron-transfer series of 1,2-benzenedithiolate,[6] and the "non-innocent" character of NO acting as NO^+, NO^- and the paramagnetic neutral NO• radical,[7] determination of the formal oxidation state of transition metal and NO in the 1,2-benzenedithiolate−metal nitrosyl complexes becomes rather complicated. Thus, the metal−NO unit is generally designated as $\{M(NO)_x\}^n$ (M = transition metal), the Enemark−Feltham notation,[8] which stresses the well-

[‡] National Tsing Hua University.
[†] National Taiwan University.
[§] National Dong Hwa University.
[⊥] National Synchroton Radition Research Center.

(1) (a) Foster, M. W.; Cowan, J. A. *J. Am. Chem. Soc.* **1999**, *121*, 4093. (b) Morse, R. H.; Chan, S. I. *J. Biol. Chem.* **1980**, *255*, 7876. (c) Reginato, N.; McCrory, C. T. C.; Pervitsky, D.; Li, L. *J. Am. Chem. Soc.* **1999**, *121*, 10217.
(2) (a) Cooper, C. E. *Biochim. Biophys. Acta* **1999**, *1411*, 290. (b) Vanin, A. F.; Stukan, R. A.; Manukhina, E. B. *Biochim. Biophys. Acta* **1996**, *1295*, 5.
(3) Cammack, R.; Joannou, C. L.; Cui, X.-Y.; Martinez, C. T.; Maraj, S. R.; Hughes, M. N. *Biochim. Biophys. Acta* **1999**, *1411*, 475.
(4) (a) Sellers, V. M.; Johnson, M. K.; Dailey, H. A. *Biochemistry* **1996**, *35*, 2699. (b) Scott, M. J.; Holm, R. H. *Angew. Chem., Int. Ed. Engl.* **1993**, *32*, 564.
(5) (a) Ford, P. C.; Bourassa, J.; Miranda, K.; Lee, B.; Lorkovic, I.; Boggs, S.; Kudo, S.; Laverman, L. *Coord. Chem. Rev.* **1998**, *171*, 185. (b) Ford, P. C.; Lorkovic, I. M. *Chem. Rev.* **2002**, *102*, 993. (c) Butler, A. R.; Megson, I. L. *Chem. Rev.* **2002**, *102*, 1155.
(6) (a) Pierpont, C. G.; Buchanan, R. M. *Coord. Chem. Rev.* **1981**, *38*, 45. (b) Attia, A. S.; Pierpont, C. G. *Inorg. Chem.* **1995**, *34*, 1172. (c) Lim, B. S.; Fomitchev, D. V.; Holm, R. H. *Inorg. Chem.* **2001**, *40*, 4257. (d) Hayton, T. W.; Legzdins, P.; Sharp, W. B. *Chem. Rev.* **2002**, *102*, 935. (e) Wang, P. G.; Xian, M.; Tang, X.; Wu, X.; Wen, Z.; Cai, T.; Janczuk, A. J. *Chem. Rev.* **2002**, *102*, 1091.
(7) (a) Franz, K. J.; Lippard, S. J. *J. Am. Chem. Soc*. **1998**, *120*, 9034. (b) Brown, C. A.; Pavlosky, M. A.; Westre, T. E.; Zhang, Y.; Hedman, B.; Hodgson, K. O.; Solomon, E. I. *J. Am. Chem. Soc.* **1995**, *117*, 715. (c) Mingos, D. M. P.; Sherman, D. J. *Adv. Inorg. Chem*. **1989**, *34*, 293.

known covalency and delocalization in the $M(NO)_x$ unit without being committed a certain formal oxidation state on either M or NO.

Recently, some interesting compounds of NO binding metal centers as $M-NO^+/M-NO^-/M-NO\bullet$ have been reported.[5,6,9−17] Lippard and co-workers reported that the Fe in complex [(NO)-Fe(TC-5,5)] (TC-5,5 = tropocoronand) adopts a trigonal bipyramidal, low-spin state with a linearly coordinated nitroxy (Fe−N−O = 174.3(4)°) group containing a short Fe−N distance of 1.670(4) Å,[9] $\{Fe^{III}(NO^-)\}$.[7] The electronic structure of $[Fe(H_2O)_5(NO)]^{2+}$ is best described as $[Fe^{III}(H_2O)_5(NO^-)]^{2+}$ in which high-spin Fe^{III} is antiferromagnetically coupled with NO^- ($S = 1$) to yield the observed spin quartet ground state ($S = {}^3/_2$).[10] Interestingly, the experimental and theoretical studies show that $[(NC)_5Fe(NO)]^{3-}$ contains delocalized oxidation levels of the metal and ligand, namely a resonance hybrid of $[(NC)_5Fe^{II}(NO\bullet)]^{3-}$ and $[(NC)_5Fe^{I}(NO^+)]^{3-}$.[11] Also, the Fe^{III} center binds NO in the form of $Fe^{II}-NO^+$, and Co^{II} binds NO in the form of $Co^{III}-NO^-$ in metmyoglobin and reduced vitamin B_{12}, respectively.[12,13]

In spite of a large number of mononuclear/tetranuclear iron−thiolate−nitrosyl complexes,[14−17] examples of trinuclear iron−NO complexes surrounded by thiolate ligands are limited.[15] By application of nitrosylation, we have prepared the mononuclear $[PPN][(ON)Fe(S,S\text{-}C_6H_4)_2]$.[17] The neutral, paramagnetic trinuclear iron−thiolate−nitrosyl complex, $[(ON)Fe(\mu\text{-}S,S\text{-}C_6H_4)]_3$ (**1**), was produced upon the protonation of the mononuclear iron−thiolate−nitrosyl $[PPN][(NO)Fe(S,S\text{-}C_6H_4)_2]$ by HBF_4 in THF. Oxidation of complex **1** in CH_2Cl_2 yields the diamagnetic trinuclear complex $[(ON)Fe(\mu\text{-}S,S\text{-}C_6H_4)]_3[PF_6]$ (**2**). Crystalline samples of complexes **1** and **2** were characterized by IR, UV−vis, ^1H NMR, EPR spectroscopy, X-ray diffraction study, magnetic susceptibility measurements, and Fe/S/N K-edge X-ray absorption spectroscopy (XAS).

Results and Discussion

Synthesis. A new member of a class of iron−sulfur−nitrosyl clusters, the neutral trinuclear Fe−thiolate−nitrosyl complex $[(ON)Fe(\mu\text{-}S,S\text{-}C_6H_4)]_3$ (**1**) containing three bridging $[S,S\text{-}C_6H_4]^{2-}$ ligands bound to three Fe's in a bidentate manner was obtained when 1 equiv of HBF_4 was added to $[PPN][(NO)Fe(S,S\text{-}C_6H_4)_2]$ in THF and stirred overnight at ambient temperature (Scheme 1a−c).[17,18] Complex **1** was isolated as a greenish brown solid. The IR spectrum of complex **1** reveals one broad absorption band for the NO groups at 1751 cm^{-1} (KBr), reflecting qualitatively the closely equivalent electronic environment of three $[Fe(NO)S_4]$ fragments.[15,17] Complex **1** exhibits a diagnostic ^1H NMR spectrum with the 1,2-benzenedithiolate proton resonances well removed from the diamagnetic region. The protons resonate upfield, 2.60 (br), −0.192 (br) ppm, which is consistent with the paramagnetic species.

Scheme 1

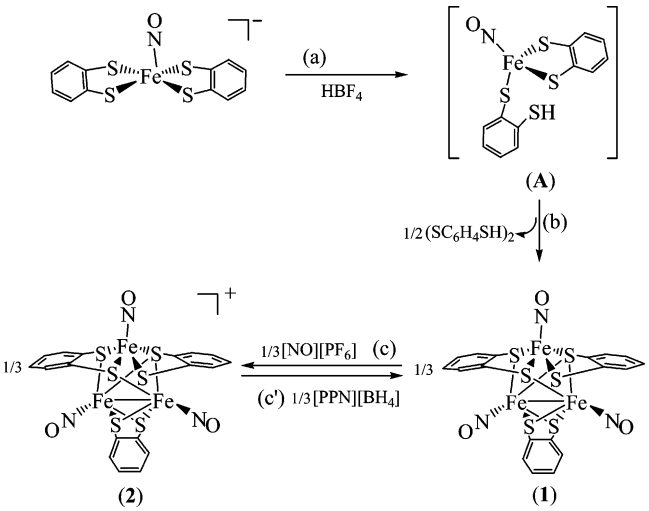

The formation of complex **1** from the protonation of $[(NO)Fe(S,S\text{-}C_6H_4)_2]^-$ can be interpreted as coordinative association of three $[(NO)Fe(S,S\text{-}C_6H_4)]$ motifs, where 1,2-benzenedithiolates served as bridging ligands between two Fe atoms. The plausible reaction path is given in Scheme 1a,b; the protonation of one dithiolate ligand of complex $[(NO)Fe(S,S\text{-}C_6H_4)_2]^-$ would yield an unstable intermediate, $[(NO)Fe(S\text{-}C_6H_4SH)(S,S\text{-}C_6H_4)]$ (**A**),[16e] which may then be accompanied by the reductive elimination of the unidentified disulfide $(S\text{-}C_6H_4SH)_2$, and presumably, the concomitant coordinative association of $[(NO)Fe(S,S\text{-}C_6H_4)]$ motifs led to the formation of **1**.

Under similar reaction conditions, oxidation of **1** by 1 equiv of $[NO][PF_6]$ in CH_2Cl_2 under N_2 at room temperature yielded a cationic trinuclear iron−thiolate−nitrosyl complex $[(ON)Fe(\mu\text{-}S,S\text{-}C_6H_4)]_3[PF_6]$ (**2**), (Scheme 1c) with each iron being ligated by four sulfur atoms as well as one nitrosyl ligand. Similar $[Fe(NO)S_4]$ motifs are found in each iron atom of **1** and **2**. In contrast to the one intense broad absorption band in the terminal nitrosyl-stretching region (IR ν_{NO}) observed in **1**, the ν_{NO} of **2** shows two discernible nitrosyl bands at 1857 cm^{-1} and 1821 cm^{-1} (KBr), which apparently shifted to higher energy from that of **1**. Similar to CO (known to serve as an indicator of electron density at iron), the shifts in ν_{NO} frequencies[17] may reflect a variation in charge on the Fe(NO) units of **2**. The ^1H NMR spectra of **2** show the expected signals (δ 7.79 (m), 7.48 (m), 6.86 (m), 6.27 (m) ppm) for the 1,2-benzenedithiolate groups' characteristics of diamagnetic species. Interestingly, **1** can be re-obtained upon chemical reduction of **2** by $[Na][BH_4]$/$[PPN][Cl]$ in 1:1 stoichiometry in CH_2Cl_2 at room temperature (Scheme 1c′). Apparently, **1** and **2** are chemically interconvertible at ambient temperature.

(8) Enemark, J. H.; Feltham, R. D. *Coord. Chem. Rev.* **1974**, *13*, 339.
(9) Franz, K. J.; Lippard, S. J. *J. Am. Chem. Soc.* **1999**, *121*, 10504.
(10) Wanat, A.; Schneppensieper, T.; Stochel, G.; van Eldik, R.; Bill, E.; Wieghardt, K. *Inorg. Chem.* **2002**, *41*, 4.
(11) Wanner, M.; Scheiring, T.; Kaim, W.; Slep, L. D.; Baraldo, L. M.; Olabe, J. A. Zalis, S.; Baerends, E. J. *Inorg. Chem.* **2001**, *40*, 5704.
(12) Laverman, L. E.; Wanat, A.; Oszajca, J.; Stochel, G.; Ford, P. C.; van Eldik, R. *J. Am. Chem. Soc.* **2001**, *123*, 285.
(13) Wolak, M.; Stochel, G.; Zahl, A.; Schneppensieper, T.; van Eldik, R. *J. Am. Chem. Soc.* **2001**, *123*, 9780.
(14) (a) Chu, C. T.-W.; Dahl, L. F. *Inorg. Chem.* **1977**, *16*, 3245. (b) Chu, C. T.-W.; Lo, F. Y.-K.; Dahl, L. F. *J. Am. Chem. Soc.* **1982**, *104*, 3409. (c) Goh, C.; Holm, R. H. *Inorg. Chim. Acta* **1998**, *270*, 46. (d) Sung, S.-S.; Glidewell, C.; Butler, A. R.; Hoffmann, R. *Inorg. Chem.* **1985**, *24*, 3856.
(15) Butler, A. R.; Glidewell, C.; Li, M.-H. *Adv. Inorg. Chem.* **1988**, *32*, 335.
(16) (a) Tsai, F.-T.; Chiou, S.-J.; Tsai, M.-C.; Tsai, M.-L.; Huang, H.-W.; Chiang, M.-H.; Liaw, W.-F. *Inorg. Chem.* **2005**, *44*, 5872. (b) Tsai, M.-L.; Chen, C.-C.; Hsu, I.-J.; Ke, S.-C.; Hsieh, C.-H.; Chiang, K.-A.; Lee, G.-H.; Wang, Y.; Liaw, W.-F. *Inorg. Chem.* **2004**, *43*, 5159. (c) Chen, H.-W.; Lin, C.-W.; Chen, C.-C.; Yang, L.-B.; Chiang, M.-H.; Liaw, W.-F. *Inorg. Chem.* **2005**, *44*, 3226. (d) Hung, M.-C.; Tsai, M.-C.; Lee, G.-H.; Liaw, W.-F. *Inorg. Chem.* **2006**, *45*, 6041. (e) Lu, T.-T.; Chiou, S.-J.; Chen, C.-Y.; Liaw, W.-F. *Inorg. Chem.* **2006**, *45*, 8799. (f) Tsai, M.-L.; Liaw, W.-F. *Inorg. Chem.* **2006**, *45*, 6583.
(17) (a) Lee, C.-M.; Hsieh, C.-H.; Dutta, A.; Lee, G.-H.; Liaw, W.-F. *J. Am. Chem. Soc.* **2003**, *125*, 11492. (b) Lee, C.-M.; Chen, C.-H.; Chen, H.-W.; Hsu, J.-L.; Lee, G.-H.; Liaw, W.-F. *Inorg. Chem.* **2005**, *44*, 6670.
(18) Hedberg, L.; Hedberg, K.; Satija, S. K.; Swanson, B. I. *Inorg. Chem.* **1985**, *24*, 2766.

Downloaded by NATIONAL TAIWAN UNIV on August 25, 2009 | http://pubs.acs.org
Publication Date (Web): January 11, 2007 | doi: 10.1021/ja065401e

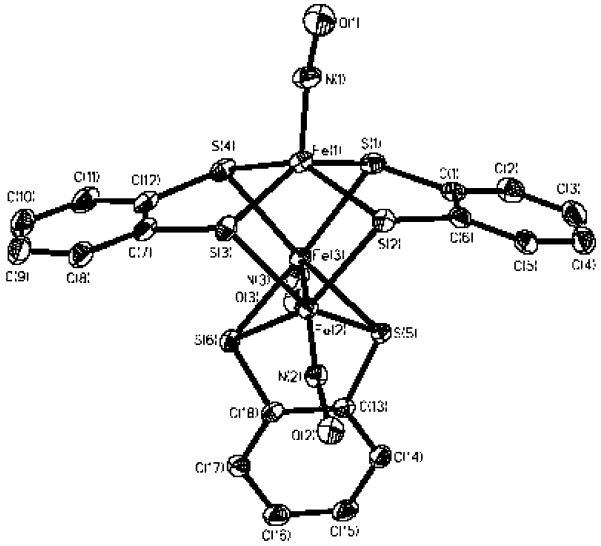

Figure 1. ORTEP drawing with 50% probability in thermal ellipsoids and labeling scheme of **1**.

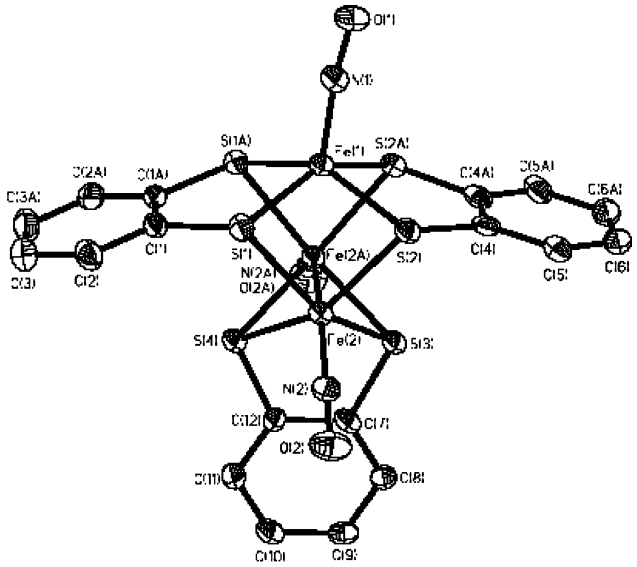

Figure 2. ORTEP drawing with 50% probability in thermal ellipsoid and labeling scheme of the cation of **2**.

Structure. The molecular structures of compound **1** and **2** were determined by single-crystal X-ray diffraction. As shown in Figures 1 and 2, **1** and **2** give a high degree of congruency. Both consist of a triangular planar Fe_3 core linked by three doubly bridged $[S,S\text{-}C_6H_4]^{2-}$ ligands, affording a core composition of Fe_3S_6. Each iron atom is five-coordinated (FeS_4N) and adopts a distorted square pyramidal geometry with a terminal NO ligand at the axial position. Each dithiolate ligand, $[S,S\text{-}C_6H_4]$, is coordinated to two iron atoms through sulfur atoms. For the convenience of discussion, we designate each Fe core (FeS_4N) as fragments 1, 2, and 3 respectively for Fe(1), Fe(2), and Fe(3). There is a crystallographic mirror symmetry passing through Fe(1) and the midpoint of the other two Fe atoms for **2**, but only a pseudo one in **1**. Bond distances around Fe atoms for both **1** and **2** are listed in Table 1. The apparently shorter Fe(2)−Fe(3) distance of 2.5779(5)Å, compared to Fe(1)−Fe(2) and Fe(1)−Fe(3) distance of 2.7820(5) and 2.7544(5)Å, respectively, indicates a greater extent of Fe(2)−Fe(3) bonding interaction in **1**. A similar observation but to less extent is also found in **2** with the Fe(2)−Fe(2A) distance of 2.569(2)Å, which is shorter than that of the Fe(1)−Fe(2) distance of 2.672(1) Å). Variations in Fe−S and Fe−N distances within the complex are not so noticeable.

Table 1. Comparison of Bond Distances (Å) around Fe Atoms in Complexes **1** and **2**

complex **1**	Å	complex **2**	Å	Δ^a (**1**–**2**) Å	Δ/σ^b
Fe(1)−Fe(2)	2.7820(5)	Fe(1)−Fe(2)	2.6724(14)	0.11	74
Fe(1)−Fe(3)	2.7544(5)	Fe(1)−Fe(3)	2.6724(14)	0.08	53
Fe(2)−Fe(3)	2.5779(5)	Fe(2)−Fe(3)	2.5694(19)	0.01	4
Fe(1)−N(1)	1.681(2)	Fe(1)−N(1)	1.646(8)	0.035	4
Fe(2)−N(2)	1.661(2)	Fe(2)−N(2)	1.648(6)	0.013	2
Fe(3)−N(3)	1.680(2)	Fe(2A)−N(2A)	1.648(6)	0.032	5
Fe(1)−S(1)	2.2536(7)	Fe(1)−S(2)	2.2236(18)	0.030	15
Fe(1)−S(2)	2.2349(7)			0.011	6
Fe(1)−S(3)	2.2614(7)	Fe(1)−S(1)	2.2361(18)	0.025	13
Fe(1)−S(4)	2.2632(7)			0.027	14
Fe(2)−S(2)	2.3223(7)	Fe(2)−S(2)	2.2781(17)	0.044	24
Fe(2)−S(3)	2.3186(7)	Fe(2)−S(1)	2.3113(18)	0.007	4
Fe(2)−S(5)	2.2660(7)	Fe(2)−S(3)	2.260(2)	0.006	3
Fe(2)−S(6)	2.2559(7)	Fe(2)−S(4)	2.2661(19)	−0.010	5
Fe(3)−S(1)	2.3335(7)	Fe(2A)−S(2A)	2.2781(17)	0.055	30
Fe(3)−S(4)	2.3150(7)	Fe(2A)−S(1A)	2.3113(18)	0.004	2
Fe(3)−S(5)	2.2562(6)	Fe(2A)−S(3)	2.260(2)	−0.004	2
Fe(3)−S(6)	2.2713(7)	Fe(2A)−S(4)	2.2661(19)	0.005	3

[a] Δ: The differences between **1** and **2** for the corresponding bond distance. [b] Δ/σ: The ratio of the differences divided by the standard deviation. The standard deviation is calculated according to the error propagation.

The particular geometrical dissimilarities found between **1** and **2** may lead to the understanding of the effects caused by the removal of one electron. Upon one-electron oxidation from **1** to **2**, bond distances of fragment 1 (around Fe(1)) are shortened the most; e.g. Fe(1)−Fe(2) and Fe(1)−Fe(3) are shortened by as much as 0.1 Å. The Fe−S distances change the most (0.03∼0.06 Å) for one of the thiolates labeled as S(1) and S(2) in Figure 1, a somewhat smaller change (∼0.025 Å) for the one labeled as S(3) and S(4), and practically no change for the one labeled as S(5) and S(6). Fe−N distances are also shortened somewhat in **2**. Detailed comparisons on other distances are listed in Table 1. This result indicates, qualitatively, that the SOMO in **1** can be identified as having antibonding character mainly in the Fe−Fe bond. Reduced electron density around the Fe_3 core and the more effective Fe−Fe interactions in **2** may also suppress the Fe−N and Fe−S antibonding interactions. Although the distance of N−O is unaccountable due to the disorder of O atoms, the significant increase in the N−O stretching frequencies in **2** does represent the shortening and strengthening of N−O bond. The geometry change around Fe(1) is obviously the biggest among three Fe atoms, indicating that the removal of the unpaired electron may take place predominantly at fragment 1. More discussion will be given later in the section of MO calculation.

Magnetic Measurement. The magnetic measurement of **1** is shown in Figure 3. It indicates that the ground state is one unpaired electron with $S_{total} = {}^1/_2$. The magnetic moment is slightly temperature dependent and could be fitted by a two-dimensional (2D) coupling model with $g = 2.01$ and $J = -0.28$. The small negative J value indicates there are weak antiferromagnetic couplings between different fragments.

X-ray Absorption Spectroscopy. The Fe K-edge absorption spectra together with some reference compounds are depicted in the Figure 4. The apparent pre-edge absorption is due to the

Downloaded by NATIONAL TAIWAN UNIV on August 25, 2009 | http://pubs.acs.org
Publication Date (Web): January 11, 2007 | doi: 10.1021/ja065401e

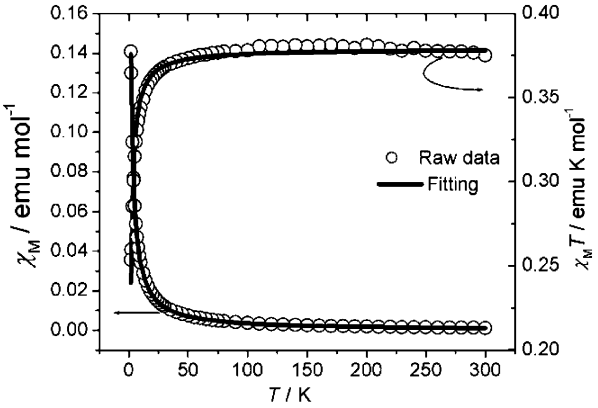

Figure 3. Magnetic measurement of **1**. χ_M and $\chi_M T$ vs T; the open circle (○) is from experimental data, and the solid line (—) is the fitted curve.

symmetry-allowed 1s to 3d transition in the distorted square pyramidal local environment of the Fe center with the d−p mixing between Fe and ligand atoms. The edge absorption is assigned to be the dipole transition from 1s to 4p orbitals of Fe. Based on the Fe K-edge absorption spectra shown in Figure 4, the formal oxidation state of Fe in **1** is definitely higher than that of Fe-foil but lower than those of FeO and Fe_2O_3. It indicates that the average oxidation state of Fe in **1** is the same as that of $(NO)Fe(S_2CNEt_2)_2$, which is generally known[19] as a nitrosyl ligand (NO^+) bonded to a low-spin d^7 Fe(I); thus, the **1** is best assigned with the average formal oxidation state of Fe(I). Take a closer look at the differences between **1** and **2** in Figure 4; the edge absorption energy of **2** is shifted only slightly to higher energy than that of **1**. Take the maximum values of the first derivative of each spectrum as the edge absorption energy; they are 7119.8 and 7120.4 eV for **1** and **2**, respectively. This may indicate that the one-electron oxidation from **1** to **2** does have a small effect on the Fe atoms.

The N K-edge absorption spectra of **1** and **2** are displayed in Figure 5. Roughly, the peaks around 400−401 and 415 eV are assigned to the transition of 1s→π* and the 1s→σ*, respectively.[20] A single peak at 400.6 eV with FWHM = 0.96 eV, and at 401.1 eV with FWHM = 0.88 eV for **1** and **2**, respectively, is assigned to be the 1s→π* transition. The single peak is an indication of NO^+ group because the NO• radical will generally give two peaks to allow the transitions of two spin states. However, one cannot completely exclude the possibility of having a small portion of the NO radical, where the unpaired electron is delocalized between Fe and NO. The slightly higher 1s→π* transition energy of **2** seems to indicate that the one-electron oxidation does have effect on the N atom of **2**. Shifting to a slightly higher energy of the 1s→π* transition position in **2** could be rationalized by the stronger bond between Fe and N of nitrosyl group due to the more positively charged Fe in 2.

The S K-edge absorption spectra of **1** and **2** are displayed in Figure 6. According to previous reports,[21] the peak around 2474 eV is assigned to be the transition of 1s(S)→π*(C−S bond), and the peak around 2471 eV is assigned to be the transition of 1s(S) to 3p(S) mixing with 3d orbital of Fe. In comparison with the 1s→3p transition of both compounds, one peak at 2471.2 eV is observed for **1**, but an additional shoulder peak at 2471.7 eV is found for **2**. However, the transition energy of 1s(S)→π*-(C−S bond) in **2** is only 0.2 eV higher than that of **1**. This seems to indicate that the one-electron oxidation does affect the Fe−S bond more than the C−S bond. This is consistent with the changes in the corresponding distances of Fe−S and S−C bonds.

According to the X-ray absorption spectra, each Fe and NO group in **1** is likely to be in the form of Fe(I) and NO^+ with the Enemark−Feltham notation of {Fe(NO)}.[7] However, according to the magnetic measurement shown in Figure 3, there is only one unpaired electron in **1** ($S_{total} = {}^1/_2$) and no unpaired electron ($S_{total} = 0$) in **2**. It is logical to assume that the oxidation takes place when this unpaired electron of complex **1** is removed from a singly occupied molecular orbital (SOMO). X-ray absorption spectra indicate that such oxidation process causes absorption edges of Fe, N, and S to be shifted slightly to higher energies. Thus, one predicts that the SOMO in complex **1** would be the combination of valence orbitals from Fe, N, and S; this result will be further confirmed by the MO calculations.

EPR/ENDOR Spectroscopy. X-band EPR spectra of the **1** frozen in CH_2Cl_2 recorded under microwave power of 2 mW and modulation amplitude of 0.1 mT at 100 kHz are shown in Figure 7. Where 7a and 7c are the spectra taken at 5 and 77 K respectively; 7d is the spectrum at 5 K on ^{15}N-labeled complex. 7b and 7e are the simulated spectra corresponding to 7a and 7d. The EPR spectra at 5 K display a rhombic symmetry with evident hyperfine splitting. This signal does not consist of a fast-relaxing component; it could still be observed at 77 K, in contrast to $[Fe_3S_4]^+$ clusters, where signals around $g = 2.01$ are only observed at temperature below 30 K. At 77 K, the hyperfine features were averaged out due to the fast tumbling of the molecule with principal g values of $g_1 = 2.011$, $g_2 = 1.999$, and $g_3 = 1.986$ (Figure 7c). There are no further signals at lower field which identifies unquestionably a spin $S = {}^1/_2$ ground state at temperature above 5 K. To clarify the origin of the observed multiline hyperfine pattern, we measured the EPR spectrum (Figure 7d) of ^{15}N-labeled **1**, wherein all the nitrogen atoms are replaced by the ^{15}N isotope (>95%). In comparison of the ^{15}N-labeled **1** with that of the naturally abundant **1** (Figure 7, spectra d and a), though the overall line shape changes are muted, changes in the number of hyperfine lines and their resonant positions clearly indicate that the electron spin is coupled to the coordinated nitrogen atoms. We have attempted to simulate the spectra of **1** for both the ^{14}N- and ^{15}N-labeled complexes based on $S = {}^1/_2$ rhombic models with two or three coordinated nitrogen atoms. A concurrent satisfactory fit to both ^{14}N- (Figure 7a) and ^{15}N- (Figure 7d) data was only obtained for a rhombic model with three nonequivalent nitrogen atoms. The simulated EPR parameters are presented in Table 2. The simulated spectra (Figure 7, spectra b and e) yield rather small

Downloaded by NATIONAL TAIWAN UNIV on August 25, 2009 | http://pubs.acs.org
Publication Date (Web): January 11, 2007 | doi: 10.1021/ja065401e

(19) (a) Goodman, B. A.; Raynor, J. B.; Symons, M. C. R. *J. Chem. Soc. (A)* **1969**, 2572. (b) Gibson, J. F. *Nature* **1962**, *196*, 64. (c) McDonald, C. C.; Phillips, W. D.; Mower, H. F. *J. Am. Chem. Soc.* **1965**, *87*, 3319.
(20) (a) Wright, G. R.; Brion, C. E. *J. Electron Spectrosc.* **1974**, *4*, 313. (b) Domke, M.; Remmers, G.; Kaindl, G. *Nucl. Instrum. Methods Phys. Res., Sect. B* **1994**, *87*, 173. (c) Stöhr, J.; Jaeger, R. *Phys. Rev. B* **1982**, *26*, 4111. (d) Kosugi, N.; Adachi, J.-I.; Shigemasa, E.; Yagishita, A. *J. Chem. Phys.* **1992**, *97*, 8842.
(21) (a) Szilagyi, R. K.; Lim, B. S.; Glaser, T.; Holm, R. H.; Hedman, B.; Hodgson, K. O.; Solomon, E. I. *J. Am. Chem. Soc.* **2003**, *125*, 9158. (b) Szilagyi, R. K.; Bryngelson, P. A.; Maroney, M. J.; Hedman, B.; Hodgson, K. O.; Solomon, E. I. *J. Am. Chem. Soc.* **2004**, *126*, 3018. (c) Glaser, T.; Rose, K.; Shadle, S. E.; Hedman, B.; Hodgson, K. O.; Solomon, E. I. *J. Am. Chem. Soc.* **2001**, *123*, 442.

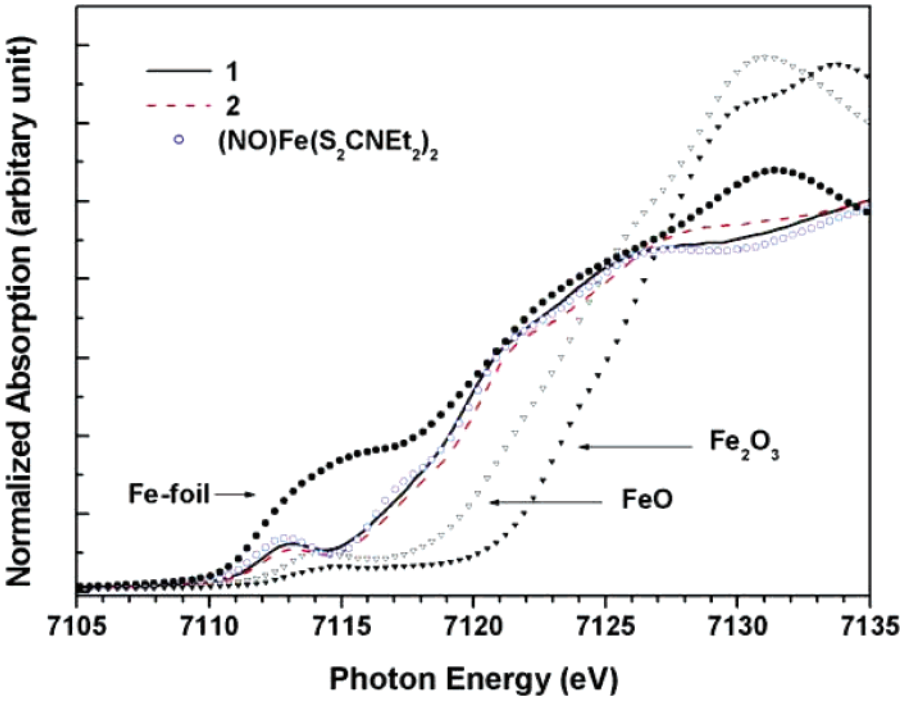

Figure 4. Fe K-edge spectra of the **1**, **2**, and some reference compounds. The solid (−) and dashed (---) lines are the **1** and **2**, respectively. The solid circle (●) Fe foil; solid triangle (▲) Fe_2O_3; open triangle (△) FeO; open circle (○) $(NO)Fe(S_2CNEt_2)_2$.

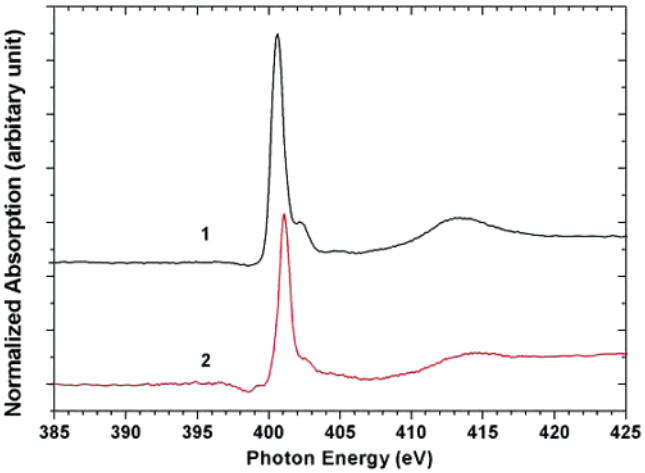

Figure 5. N K-edge spectra of the **1** (top) and **2** (bottom).

g-tensor anisotropy with principal g values of $g_1 = 2.011$, $g_2 = 1.999$, and $g_3 = 1.981$ which are consistent with the measured values at 77 K. Thus, it points to a NO $2\pi^*$-based SOMO in **1**. But, a comparison with EPR data for free nitric oxide absorbed on the surface of MgO ($g_{\|} = 1.89$, $g_{\perp} = 1.996$, $A_{\perp} = 33$ G) and ZnO ($g_{\|} = 1.94$, $g_{\perp} = 1.979$, $A_{\perp} = 30$ G) reveals a significant reduction of the NO intrinsic hyperfine coupling constants in complex **1**. This suggests that the odd electron which might be originated on fragment 1 as an NO radical is not only confined to the NO ligand but is also delocalized through the overlaps of Fe (3d) and NO ($2\pi^*$) orbitals. The unpaired electron thus possesses metal d orbital characters enhancing the spin−lattice relaxation rate and results in the vanishing of the EPR signal at a temperature approximately about 120 K. The observed nitrogen hyperfine couplings of fragments 2 and 3 are also attributed to the unpaired spin density delocalization originating from the Fe(NO) of fragment 1.

The EPR results thus lead to a favorable description of {Fe−NO} in fragment 1 as $S_1 = {}^1/_2$, possibly $\{Fe^{II}(\bullet NO)\}^7$ and $\{Fe^{I}(NO)^+\}$,[7] while fragments 2 and 3 are described as $S_{2,3} = {}^1/_2$, mainly $\{Fe^{I}(NO)^+\}$,[7] and are antiferromagnetically coupled with each other to give a $S_{total} = {}^1/_2$ ground state where all the Fe are in the low-spin state. This is imposed by the EPR results and a shorter distance between Fe atoms of fragments 2 and 3 (∼2.578 Å) compared to those of fragment 1 and 2 (∼2.782 Å) and fragment 1 and 3 (∼2.754 Å). Therefore, three different nitrogen atoms means a predominate NO radical of $\{Fe^{II}(\bullet NO)\}^7$, a nitrosyl NO^+ of $\{Fe^{I}(NO)^+\}^7$, and a form between these two. It is unlikely to assume $S = {}^3/_2$ state for any one fragment, since this requires all three fragments to coupled together in order to give a $S_{total} = {}^1/_2$ ground state and that generally results in a much faster relaxation rate.

Additional evidence that supports delocalization of the unpaired electron spin density over the whole complex framework may come from measurements of the proton ENDOR spectra. In systems of low g anisotropy, magnetically coupled protons are expected to produce ENDOR features mirrored about the free proton Larmor frequency $\nu_N = g_H\beta_N H_o/h$ (14.675 MHz at 3446.5 G) and displaced by half of the value of the hyperfine coupling constants ($\nu_{\pm}^N = \nu_N \pm A^N/2$). Figure 8 presents an expanded proton ENDOR spectrum of **1** frozen in CH_2Cl_2 recorded at 5 K under 2 mW microwave power and 40 W RF power. Hyperfine coupling in the matrix region (<1 MHz) is shown in the inset of Figure 8. The prominent feature located at the Larmor frequency of the free proton with a nominal coupling of ∼0.5 MHz is generally observed in solid-state ENDOR for close protons and is due mainly to dipolar interactions between the unpaired electron and surrounding solvent protons. The spectrum was recorded at a magnetic field

Downloaded by NATIONAL TAIWAN UNIV on August 25, 2009 | http://pubs.acs.org
Publication Date (Web): January 11, 2007 | doi: 10.1021/ja065401e

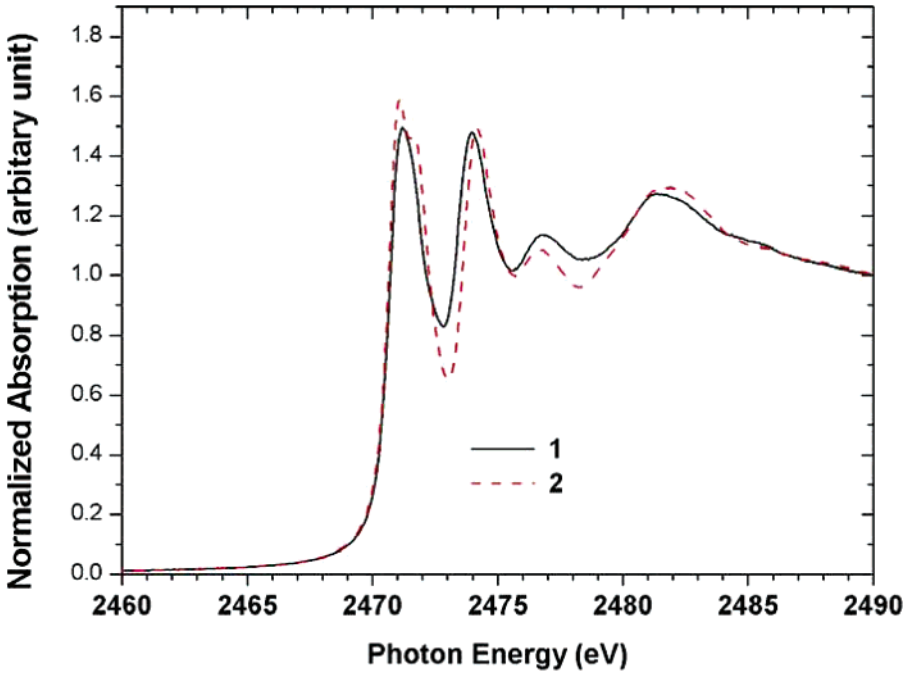

Figure 6. S K-edge spectra of the **1** (solid line) and **2** (dash line).

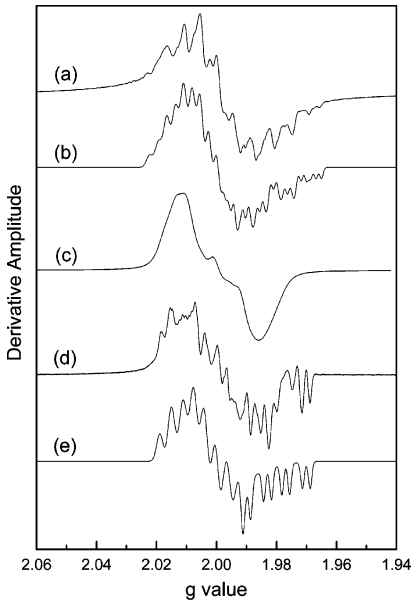

Figure 7. X-band EPR spectra and simulation of **1** frozen in CH_2Cl_2. Experimental spectra (a), (c), and (d) were obtained with a microwave power of 2 mW and modulation amplitude of 0.1 mT at 100 kHz. (a) natural abundant **1** at 5K and 9.5151 GHz microwave frequency; (b) simulation of (a); (c) natural abundant **1** at 77 K and 9.4312 GHz; (d) ^{15}N labeled **1** at 5 K and 9.520 GHz; (e) simulation of (d).

corresponding to $g = 1.999$ where all directions of space contribute to the maximum of the EPR envelope. Therefore, ENDOR transitions (labeled as a−a′, b−b′, and c−c′ through f−f′) caused by intensity buildup correspond to principal values of hyperfine tensors of the benzene ring protons that are coupled to the delocalized unpaired spin density. Table 3 lists the ring protons hyperfine coupling constants given by the frequency separation between pairs of features that appear symmetrically about the ^1H Larmor frequency. These weak transitions are best observed at temperature below 20 K and under conditions of high RF modulation and power which enhance the signal-to-noise ratio at the expanse of spectral resolution.

Table 2. Principal Hyperfine Coupling Constants and Directions of the *g* and ^{14}N Hyperfine Tensors for Complex **1**

	principle values	Euler angles[a]
g-tensor	(2.011, 1.999, 1.981)	
hyperfine tensor (Gauss)		
fragment 1 (Fe(1)−N(1)−O(1))	(9.2, 6.6, 15.6)	(6, −150, 18)
fragment 2 (Fe(2)−N(2)−O(2))	(3.3, 9.4, 1.9)	(96, −86, 63)
fragment 3 (Fe(3)−N(3)−O(3))	(7, 1, 3.6)	(70, 5, −32)

[a] Euler angles, in (deg), are defined as in Goldstein (Goldstein, H. *Classical Mechanics*; Addison Wesley: Reading MA, 1967).

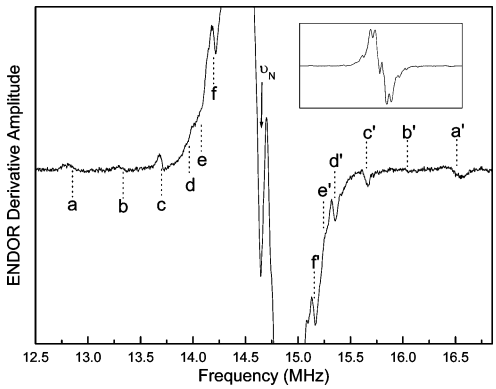

Figure 8. Proton ENDOR spectra of **1** frozen in CH_2Cl_2. The spectrum was taken at the maximum EPR absorption corresponding to $g = 1.999$ of Figure 7. The ^1H Larmor frequency (ν_N) is 14.675 MHz. Conditions: microwave frequency 9.6427 GHz; $H_o = 3446.5$ G; microwave powder, 2 mW; radio frequency power, 40 W; FM amplitude, 20 kHz; number of scans, four; temperature, 5 K. Six different ^1H doublets (labeled as a−a′, b−b′, and c−c′ through f−f′) are seen split symmetrically about ν_N.

Tentative assignments of the ring α-protons hyperfine tensors are made by comparison with the magnitude and apportioning the principal values given in Table 3 according to established physical models. For α-protons, one expects a rhombic principal hyperfine tensor component pattern of $0.5a_{iso}$, $1.0a_{iso}$, and $1.5a_{iso}$

Downloaded by NATIONAL TAIWAN UNIV on August 25, 2009 | http://pubs.acs.org
Publication Date (Web): January 11, 2007 | doi: 10.1021/ja065401e

Table 3. Proton Hyperfine Coupling Constants and Assignments for Complex **1** Determined by CW-ENDOR

transitions	hyperfine constants (MHz)	assignments protons bonded to
a, a′	$A_X = -3.66$	C (2,5,8,11)
b, b′	$A_Z = -2.69$	C (2,5,8,11)
c, c′	$A_X = -1.93$	C (3,4,9,10)
d, d′	$A_Z = -1.33$	C (3,4,9,10)
e, e′	$A_Y = -1.23$	C (2,5,8,11)
f, f′	$A_Y = -0.88$	C (3,4,9,10)

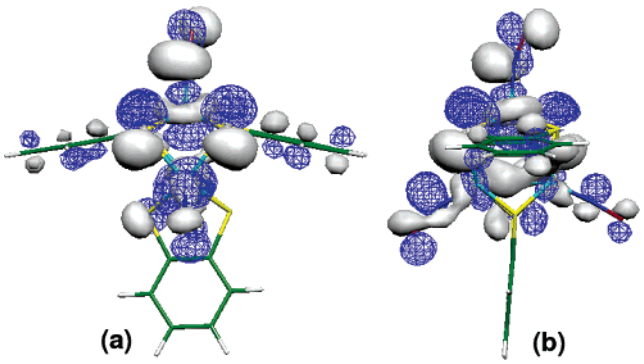

Figure 9. Wave function of SOMO of **1,** view (a) along the pseudo-mirror; (b) perpendicular to (a).

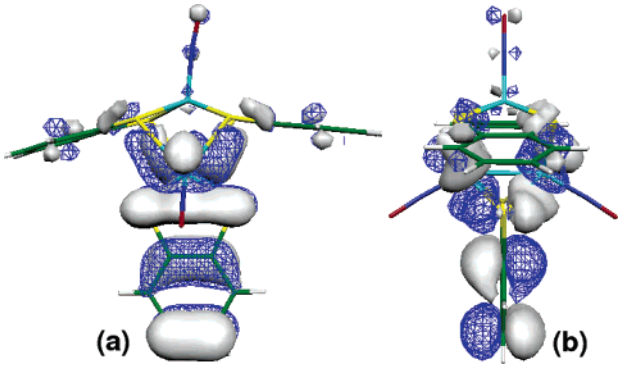

Figure 10. Wave function of HOMO of the cation of **2**, view (a) along the mirror; (b) perpendicular to (a).

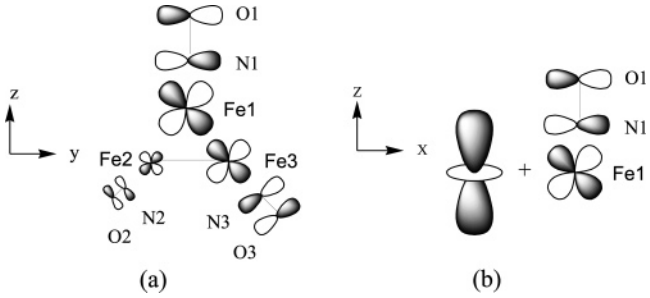

Figure 11. Some important orbital coefficients of SOMO at (a) $Y-Z$ plane (b) $X-Z$ plane. The selected SOMO coefficients are listed in the Supporting Information.

that are along the C−H bond (A_Y), parallel to the axis of the p_z orbital (A_Z), i.e., normal to the benzene ring, and perpendicular to the C−H bond (A_X), respectively. According to this rule, the grouping of observed hyperfine couplings into the A_X, A_Y, and A_Z components for two sets of distinguishable protons are presented in Table 3. Also, for α-protons, we expect that the sign of the isotropic hyperfine coupling will be negative. The hyperfine tensors obtained from the ENDOR transition frequencies are in good correspondence with the physical model for α-protons. We therefore make the assignments of these ENDOR features of the benzene ring protons, and that establishes the spin delocalization picture of fragment 1 of **1**.

MO Calculation. Both unrestricted and restricted open shell MO calculations of **1** have been performed by taking the geometry from the respective crystal structure. The overall results are roughly the same. The unrestricted one yields the expectation value of total spin quantum number,[22] $\langle S^2 \rangle$, of 0.78, which is close to the ideal eigenvalue of 0.75 with $S = {}^1/_2$. The atomic charge analysis gives about the same charge on each iron atom of **1**, no matter what types of atomic partition is taken into account. The calculated principal g-values, $g_1 = 2.011$, $g_2 = 1.993$, and $g_3 = 1.983$, at ground state are in good agreement with the ones derived from EPR. The SOMO of **1** is depicted in Figure 9, where the major contribution is obviously from the fragment 1 with Fe(1) and its associated ligands, some contributions from Fe-(NO) of fragment 2 and 3. Thus the unpaired electron of **1** is mainly located on the fragment 1, {(NO)Fe(1)($S_2C_6H_4$)}, but only partially delocalized to the other two Fe(NO) parts. On the contrary, the highest occupied molecular orbital (HOMO) of **2** is principally contributed from d-orbitals of Fe2 and Fe3 and only slightly from the fragment 1 as shown in Figure 10. In fact, it is quite similar to the orbital next (lower energy) to the SOMO in **1**. Detailed analysis of the coefficients of SOMO reveals that the orbital is predominately contributed from fragment 1 including Fe(1)−N(1)−O(1) and the sulfur atoms of two thiolates; roughly 30%, 12%, and 21% for Fe, NO, and S, respectively. The other important contribution comes from Fe(3)−N(3)−O(3) where 13% and 8% from Fe(3) and N(3)O(3), respectively. The large coefficients are all from d-orbitals of Fe and π^* orbitals of NO; this means the unpaired electron is delocalized among Fe atoms and NO ligands through d−d and d−π^* interactions. The most important part of interatomic interactions of SOMO are depicted in Figure 11. It is obvious that the d−p π^* characters between Fe(1) and N(1) are in antibonding character with both d_{yz} and d_{xz} of Fe. In addition, all the NO bonds are also in antibonding character. More importantly, the biggest coefficient in SOMO is on the d_{z^2} of Fe(1) which amounts to 23% of contribution. The removal of one electron from such an orbital yields the shortening and strengthening of the NO bond with much higher ν_{NO} stretching frequency in **2**. It also yields the shortening of Fe−N bond. However, the shortening of Fe−Fe distances is not so straightforward due to many d−d interactions; some are bonding, the others are antibonding. The coefficients are, in general, very large, indicating that the unpaired electron does locate predominately on the Fe atoms, especially Fe(1), which gives the confirmation of having low-spin d^7 Fe(I) observed from XAS. The three possible different forms of NO deduced from the hyperfine splittings of EPR spectra are realized to be corresponding to NO radical, NO^+, or a resonance hybrid. The π^*_{NO} is always overlapped with Fe d-orbitals as shown in Figure 11,

(22) (a) Bulo, R. E.; Ehlers, A. W.; Grimme, S.; Lammertsma, K. *J. Am. Chem. Soc.* **2002**, *124*, 13903. (b) For calculating the $\langle S^2 \rangle$ values, the following formula was implemented in the ADF algorithm: $\langle S^2 \rangle_{uhf} = \langle S^2 \rangle_{exact} + N^\beta - \sum_i^N \sum_j^N |S_{ij}^{\alpha\beta}|$ and $\langle S^2 \rangle_{exact} = [(N^\alpha - N^\beta)/2]\,[(N^\alpha - N^\beta)/2 + 1]$. S_{ij} is the overlap integral of α-orbital i with β-orbital j, and N is the number of electrons where $N^\alpha \geq N^\beta$. See: Szabo, A.; Ostlund, N. S. *Modern Quantum Chemistry*, 1st revised ed.; McGraw-Hill: New York, 1989; p 107.

Downloaded by NATIONAL TAIWAN UNIV on August 25, 2009 | http://pubs.acs.org
Publication Date (Web): January 11, 2007 | doi: 10.1021/ja065401e

the symbol of {Fe(NO)}^{7} speaks well of such spin delocalization character in this complex. However, the calculated spin densities at Fe(1), Fe(2), and Fe(3) are 0.60, −0.15, and 0.25, respectively, whereas at N(1), N(2), and N(3) the spin densities are only 0.04, 0.02, and 0.05.

Conclusion

The neutral trinuclear Fe−thiolate−nitrosyl **1** was obtained from the protonation of a mononuclear complex [PPN][(NO)Fe(S,S-C_6H_4)$_2$], and **2** was subsequently obtained by the oxidation of **1**. The coordination environment of [FeS_4(NO)] units remains intact when **1** was oxidized to yield **2**; however, all of the Fe−Fe, Fe−N, and Fe−S distances are shortened significantly, especially around Fe(1). Taking the results from X-ray diffraction, X-ray absorption, magnetic measurement, EPR measurement, and the MO calculation, each [Fe(NO)] moiety of **1** is best described as {Fe(NO)},^{7} i.e. an unpaired electron delocalized between Fe and NO via d−π^* interaction. No evidence of any possibility of quartet ground state ($S = {}^3/_2$) existed based on magnetic and EPR measurements; each iron is mainly in a low-spin d^7 Fe^I, but Fe(2) and Fe(3) are antiferromagnetically coupled with each other. Due to the change of geometry upon one-electron oxidation of **1** to **2**, and based on the wavefunction of the SOMO of **1**, the unpaired electron in **1** is, presumably, delocalized among three [Fe(NO)] moieties together with the two bidentate dithiolates of Fe(1), but with the majority of contribution coming from the Fe(1) fragment. The SOMO is mainly contributed from the d−p π^* overlap between Fe and N or S. However, the d−d interactions between the Fe atoms gives a net antibonding character between Fe(1) and Fe(2) or Fe(1) and Fe(3). Indeed, the geometry around the Fe(1) changes the most from **1** to **2** when the removal of the unpaired electron is exercised. The spin density is indeed allocated predominately on Fe atoms.

Experimental Section

Manipulations, reactions, and transfers of samples were conducted under nitrogen according to standard Schlenk techniques or in a glovebox (argon gas). Solvents were distilled under nitrogen from appropriate drying agents (methylene chloride, diethyl ether, and methanol from CaH_2, acetonitrile from CaH_2-P_2O_5, hexane and tetrahydrofuran (THF) from sodium benzophenone) and were stored in dried, N_2-filled flasks over 4 Å molecular sieves. Nitrogen was purged through these solvents before use. Solvent was transferred to a reaction vessel via a stainless steel cannula under positive pressure of N_2. The reagents iron pentacarbonyl, sodium nitrite, 1,2-benzenedithiol, bis(triphenylphosphoranylidene)ammonium chloride, fluoroboric acid, sodium borohydride (Lancaster/Aldrich) were used as received. Complex [PPN][$Fe(CO)_3$(NO)] was synthesized and characterizd by published procedures.[18] Infrared spectra of the ν(NO) stretching frequencies were recorded on a Perkin-Elmer model spectrum one B spectrophotometer with sealed solution cells (0.1 mm) and KBr windows. Hewlett-Packard 71 and GBC Cintra 10e spectrophotometers were used to record the UV−vis spectra of each complex. ^{1}H NMR spectra were recorded on a Bruker model AC 200 spectrometer. Analyses of carbon, hydrogen, and nitrogen were obtained with a CHN analyzer (Heraeus).

Preparation of [(ON)Fe(μ-S,S-C_6H_4)]$_3$ (1). HBF_4 (73 μL, 0.6 mmol) was slowly added to the THF (10 mL) solution of [PPN][(NO)Fe(S,S-C_6H_4)$_2$] (0.611 g, 0.6 mmol)[17] by syringe, and the mixture stirred for 2 h at ambient temperature. The color of the reaction solution changed from red brown to greenish brown. The reaction was then monitored with FTIR. The IR spectrum (ν_{NO}: 1760 cm^{-1}(THF)) was assigned to the formation of neutral [(ON)Fe(μ-S,S-C_6H_4)]$_3$ (**1**) (0.163 g, 40%). Diethyl ether was then added to the solution and filtered through Celite to remove the white insoluble solid. The filtrate (THF−diethyl ether mixture) stood at −15 °C for 4 weeks and led to greenish brown crystals suitable for single-crystal X-ray diffraction. IR (ν_{NO}): 1760 br cm^{-1} (THF); 1751 br cm^{-1} (KBr). ^{1}H NMR ($CDCl_3$): δ 2.61 (br), −0.192 (br) ppm (C_6H_4). Absorption spectrum (CH_2Cl_2) [$\lambda_{max,\ nm}$ (ϵ, M^{-1} cm^{-1})]: 303 (33556), 357 (21556), 408 (16455) 589 (2466). Anal. Calcd for $C_{18}H_{12}O_3N_3S_6Fe_3$: C, 31.88; H, 1.78; N, 6.20. Found: C, 32.56; H, 1.89; N, 5.83.

Preparation of [(ON)Fe(μ-S,S-C_6H_4)]$_3$[PF_6] (2). Compound **1** (0.407 g, 0.6 mmol,) and [NO][PF_6] (0.105 g, 0.6 mmol,) were loaded in a flask and dissolved in 10 mL of CH_2Cl_2. The mixture was then stirred for 1 h. The color of the solution changed from greenish brown to dark green. The reaction was monitored afterward with FTIR immediately. IR spectrum (ν_{NO}: 1836, 1857 cm^{-1}(CH_2Cl_2)) corresponds to the formation of **2** (0.286 g, 58%). The solution was filtered through Celite, and then diethyl ether was added to precipitate the dark-green solid. Diffusion of hexane−diethyl ether into a saturated CH_2Cl_2−MeOH solution of **2** at −15 °C gave dark-green crystals suitable for single-crystal X-ray diffraction. IR (ν_{NO}): 1836, 1857 cm^{-1} (CH_2Cl_2) 1821, 1857 cm^{-1} (KBr). ^{1}H NMR ($CDCl_3$): δ 7.80 (m), 7.48 (m), 6.86 (br), 5.28 (br) ppm (C_6H_4). Absorption spectrum (CH_2Cl_2) [λ_{max}, nm (ϵ, M$^{-1\ cm-1}$)]: 351 (32857), 402 (21950), 572 (4245). Anal. Calcd for $C_{18}H_{12}PFe_3N_3O_3S_6F_6$: C, 26.26; H, 1.47; N, 5.10. Found: C, 27.61; H, 2.00; N, 5.28.

Reduction of [(ON)Fe(μ-S,S-C_6H_4)]$_3$[PF_6]. A CH_2Cl_2 solution (6 mL) containing 0.329 g (0.4 mmol) of **2**, 0.151 g (0.4 mmol) of [Na][BH_4], and 0.229 g (0.4 mmol) of [PPN][Cl] was stirred at ambient temperature for 1 h. The color of the solution changed from dark green to greenish brown. Diethyl ether (6 mL) was added to the solution, and then the mixture was filtered through Celite to remove the insoluble solid. The filtrate (CH_2Cl_2−diethyl ether mixture) was then dried under vacuum to obtain green-brown solid. The IR (ν_{NO}: 1760 br (THF); 1751 br cm^{-1} (KBr)), UV−vis (absorption spectrum (CH_2Cl_2) [$\lambda_{max,\ nm}$]: 303, 357, 408, 589) and ^{1}H NMR spectrum (δ 2.61 (br), −0.19 (br) ppm (C_6H_4) ($CDCl_3$)) indicated the formation of **1**.

Magnetic Measurements. The magnetization data were recorded on a SQUID magnetometer (MPMS XL Quantum Design company) with an external magnetic field of 1.0 T in the temperature ranges of 2−300 K. The experimental magnetic susceptibility data were corrected for diamagnetism.

X-ray Absorption Spectroscopy. All X-ray absorption experiments were carried out at the National Synchrotron Radiation Research Center (NSRRC), Hsinchu, Taiwan. All spectra were recorded at room temperature. For Fe K-edge measurements, the experiment was performed in transmission mode at the BL-17C wiggler beamline with a double crystal monochromator of Si(111). The energy resolution $\Delta E/E$ is 2×10^{-4}. High harmonics were removed by using Rh-coated mirrors. The energy is scanned from 6.912 to 8.105 KeV using a gas-ionization detector. A reference Fe foil is always used as an internal standard for the calibration of energy. The ion chambers used to measure the incident (I_0) and transmitted (I) intensities were filled with a mixture of N_2 and He gas and a mixture of N_2 and Ar gas, respectively.

The S K-edge data were measured in fluorescence mode at BL-15B DCM with Si(111). The energy resolution $\Delta E/E$ is 1.4×10^{-4}. The energy is scanned from 2.4 to 3.0 KeV using Lytle detector in fluorescence mode. The sample chamber is filled with high purity-He gas to avoid the air absorption. Samples were ground to powder from single crystals, and secured onto a piece of cellophane tape. The photon energy was calibrated to the maximum of the first preedge feature of $Na_2S_2O_3$·$5H_2O$ at 2472.02 eV.

For N K-edge absorption, the data were collected at the 6-m high-energy spherical grating monochromator (HSGM) beamline with 10×10 μm opening slits, corresponding to ~0.08 eV energy resolution. Samples were ground to powder from single crystals, then secured onto conducting tape, and subjected to an ultrahigh vacuum chamber (10^{-9}

Downloaded by NATIONAL TAIWAN UNIV on August 25, 2009 | http://pubs.acs.org
Publication Date (Web): January 11, 2007 | doi: 10.1021/ja065401e

Torr). The spectra were recorded in total electron yield mode with a microchannel plate as detector. Each spectrum was calibrated by using the known absorption at 531.3 eV of Cr oxides.

EPR/ENDOR Measurements. EPR measurements were performed at X-band using a Bruker EMX spectrometer equipped with a Bruker TE102 cavity. The microwave frequency was measured with a Hewlett-Packard 5246L electronic counter. During EPR measurements, the temperature was maintained at 5 K by using an Advanced Research System Helitran continuous flow cryostat (3.2−200 K) or at 77 K by immersion of the EPR sample tube into liquid nitrogen containing a finger Dewar. The EPR instrument settings are shown in the figure legend. ENDOR spectra were recorded with a Bruker DICE ENDOR assembly equipped with a Bruker TM_{110} ENDOR cavity fitted with a home-built RF coil for introducing the RF radiation in conjunction with a high-power RF amplifier (ENI 3200L) to generate the CW B_2 field in the cavity. ENDOR spectra were collected in frequency modulation mode by stepping the RF frequency over the range from 0.5 to 50 MHz. The ENDOR instrument settings are shown in the figure legend.

MO Calculation. DFT calculations were carried out by Amsterdam Density Functional 2004.01 (ADF)[23] with the generalized gradient approximation (GGA). The corrections of LDA and GGA parts are taken fromVWN[24] and BP.[25,26] The SCALAR ZORA is used for relativistic corrections. A close shell MO calculation of the cation of **2** is performed. Both unrestricted and restricted open shell MO calculations of **1** have been computed. The triple-ζ Slater type function complemented with two polarization functions (TZ2P) are used for all atoms. Geometric coordinates of each complex were taken from the single-crystal structure. The coordinate system employed is such that the origin is set at the Fe(1) atom; the *z*-axis is collinear with Fe(1)−N(1) bond; the *x*-axis is perpendicular to *z*-axis and at the bisection of ∠S(1)−Fe−S(2). Atomic positions of N and O atoms are optimized due to the uncertainty in the crystal data. The optimization criteria are as following: (i) the difference in the total energy between two successive cycles has to be less than 0.001 hartree; (ii) the maximal difference in the norm of the gradient between two successive cycles has to be less than 0.01 hartree/Å; (iii) the maximal difference in the Cartesian coordinate between two successive cycles has to be less than 0.01 Å.

X-ray Diffraction. Crystallographic data and the detailed atomic parameters of complexes **1** and **2** are summarized in the Supporting Information (Table S1). The crystals of **1** and **2** chosen for X-ray diffraction studies are measured in size 0.28 mm × 0.28 mm × 0.10 mm, and 0.18 mm × 0.16 mm × 0.09 mm, respectively. Each crystal was mounted on a glass fiber and quickly coated in epoxy resin. Unit cell parameters were obtained by least-squares refinement. Diffraction measurements for **1** and **2** were carried out on a SMART CCD diffractometer with graphite-monochromated Mo Kα radiation (λ = 0.7107 Å) and θ between 1.84° and 27.50° for **1**, and between 1.59° and 27.50° for **2**. Least-squares refinement of the positional and anisotropic thermal parameters of all non-hydrogen atoms and fixed hydrogen atoms was based on F^2. A SADABS[27] absorption correction was made. The SHELXTL[28] structure refinement program was employed. In the case of **1**, the oxygen atoms in all NO groups were found to be disordered, two positions were modeled in 50% each with positional coordinates refined.

Acknowledgment. We thank the National Science Council (Taiwan) for the financial support of this work. We also thank NSRRC and NCHC for their support on the hardware and software applied in this work.

Supporting Information Available: X-ray crystallographic files in CIF format for the structural determinations of complexes **1** and **2**, include crystallographic data, refinement parameters, and bond distances/angles; crystallographic data of complexes **1** and **2**, the SOMO coefficients and compositions of the selected atomic orbitals of SOMO, Tables S1, S2, and S3, respectively. This material is available free of charge via the Internet at http://pubs.acs.org.

JA065401E

(23) (a) teVelde, G.; Bickelhaupt, F. M.; van Gisbergen, S. J. A.; Guerra, C. F.; Baerends, E. J.; Snijders, J. G.; Ziegler, T. *J. Comput. Chem*. **2001**, *22*, 931. (b) Fonseca Guerra, C.; Snijders, J. G.; teVelde, G.; Baerends, E. J. *Theor. Chim. Acta* **1998**, *99*, 391.
(24) Vosko, S. H.; Wilk, L.; Nusair, M. *Can. J. Phys.* **1980**, *58*, 1200.
(25) Becke, A. D. *Phys. Rev. A* **1988**, *38*, 3098.
(26) Perdew, J. P.; Yang, W. *Phys. Rev. B* **1986**, *33*, 8800.
(27) Sheldrick, G. M. *SADABS, Siemens Area Detector Absorption Correction Program*; University of Göttingen: Germany, 1996.
(28) Sheldrick, G. M. *SHELXTL, Program for Crystal Structure Determination*; Siemens Analytical X-ray Instruments Inc.: Madison, WI, 1994.

Downloaded by NATIONAL TAIWAN UNIV on August 25, 2009 | http://pubs.acs.org
Publication Date (Web): January 11, 2007 | doi: 10.1021/ja065401e